Analytical prediction model for non-symmetric fatigue crack growth in Fibre Metal Laminates

Wang, Wandong; Rans, Calvin; Benedictus, Rinze

DOI
10.1016/j.ijfatigue.2017.06.035

Publication date
2017

Document Version
Accepted author manuscript

Published in
International Journal of Fatigue

Postprint of International Journal of Fatigue
Volume 103, October 2017, Pages 546-556
Link to formal publication (Elsevier): https://doi.org/10.1016/j.ijfatigue.2017.06.035

Analytical prediction model for non-symmetric fatigue crack growth in Fibre Metal Laminates

Wandong Wang[a,*], Calvin Rans[a], Rinze Benedictus[a]

[a]*Structural Integrity & Composites Group, Faculty of Aerospace Engineering, Delft University of Technology, P.O. Box 5058, 2600 GB Delft, The Netherlands*

Abstract

This paper proposes an analytical model for predicting the non-symmetric crack growth and accompanying delamination growth in FMLs. The general approach of this model applies Linear Elastic Fracture Mechanics, the principle of superposition, and displacement compatibility based on the understanding of deformation behaviour in eccentrically cracked metal panels. The non-symmetric crack growth behaviour of two crack tips and accompanying asymmetric load transfer from the eccentrically cracked metal layers to the intact bridging fibres are successfully predicted with the model. The predicted crack growth rates and delamination evolution are compared to test data, good correlation is observed.

Keywords: non-symmetric crack, fibre metal laminates, crack opening displacement, stress intensity factor

1. Introduction

Fibre Metal Laminates (FMLs) are composed of alternating metallic layers and fibre-reinforced polymer layers. The fatigue resistant fibre layers remain intact in the wake of fatigue cracks in metal layers in FMLs under cyclic loading, restraining the crack opening and acting as a second load path for the cracked metal layers. This bridging mechanism, shown in Fig. 1, dramatically reduces the stress severity at the crack tip and thus the crack growth in metal layers [1–4]. One variant of FMLs, Glare, has been successfully applied as fuselage skin material on Airbus A380. Its superior damage tolerance in comparison with monolithic metal panels significantly contributes to the successful application.

Alderliesten has studied symmetric crack growth in FMLs under Mode I fatigue loading based on Linear Elastic Fracture Mechanics (LEFM) [2, 3]. The fatigue damage mechanisms in FMLs involve fatigue crack growth in the metal layers and accompanying delamination at metal/composite interfaces. These two coupled damage mechanisms are investigated by Alderliesten through applying the principle of superposition and estimating the load transfer between the cracked metal layers and intact fibre layers with the principle of displacement compatibility. The load transfer can be attributed to the fact that the intact bridging fibres restrain the crack opening in the metal layers, which reduces the stresses experienced at the crack tip and introduces interface delamination. The Alderliesten model has been refined for variable amplitude loading [5–7] and for part-through cracks [8].

One limitation of the Alderliesten model is that it cannot be applied to analyse non-symmetric crack cases in FMLs. However, non-symmetric fatigue crack cases can arise in FMLs in practice for several reasons, such as the scatter of crack initiation at hole edges and crack interaction in case of Multiple-site Damage (MSD) scenario [10] etc. One tip of a non-symmetric crack can grow faster than the other tip under fatigue loading. Therefore a prediction model is needed to extend the ability to analyse non-symmetric crack growth behaviour in FML structures, which is required to meet the damage tolerance requirement. In addition,

*Corresponding author. *Tel.:* +31 (0)15 278 9748;
E-mail address: w.wang-3@tudelft.nl, wwandong@gmail.com

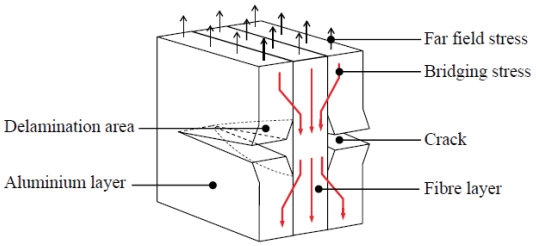

Figure 1: Illustration of bridging mechanism [9]

another motivation for developing such a model is to analyse MSD crack growth behaviour in FMLs [10, 11]. As a result of crack interaction in an FML with MSD, a single crack may have asymmetric configuration involving crack tip asymmetry and delamination asymmetry (see Fig. 2). The ability to calculate the non-symmetry effects on the states of a single crack, such as stress intensity factors and load transfer between cracked metal layers and intact bridging fibres, in an FML is therefore needed. The effects of adjacent MSD cracks on the state of the single crack in an FML can be estimated with the load redistribution mechanism according to the philosophy in [10, 11]. All crack states can be calculated by analysing each single crack in an FML with MSD scenario [10, 11].

Many attempts to address non-symmetric crack growth in finite metallic structures can be found in open literature [12–19], but no analytical prediction model for non-symmetric crack growth in FMLs has been found in open literature. One obstacle for developing such an analytical model is to understand the deformation behaviour of an eccentrically cracked panel. The crack opening displacement of a non-symmetric crack is of particular importance in analysing the load transfer between the cracked layers to intact bridging fibres in an FML.

This paper proposes an analytical model for predicting the fatigue crack growth of non-symmetric cracks in FMLs. The model is built upon the success of Alderliesten by applying LEFM, the principles of superposition and displacement compatibility. The implications of non-symmetry on fatigue cracking behaviour in FMLs are highlighted in comparison with the symmetric crack scenario in Section 2. The model development is detailed in Section 3 with focuses on the analysis of non-symmetry effects on stress intensity factors and crack opening displacement, and on the analysis of non-symmetric bridging calculation. Section 5 provides the validation of the proposed model with the test program detailed in Section 4.

2. Comparison of symmetric and non-symmetric crack growth behaviour in FMLs

In FMLs, fatigue crack growth in metal layers and delamination propagation at composite/metal interfaces take place simultaneously and interact with each other through the bridging mechanism. The growth behaviour of the two crack tips is affected not only by the free edge boundary conditions, but also the difference in delamination shapes for the tips. A symmetric fatigue crack configuration in an FML means crack tip symmetry (same boundary conditions) and delamination symmetry (no difference in delamination shapes for two crack tips), illustrated in Fig. 2(a). A non-symmetric crack configuration can be either delamination asymmetry (Fig. 2(b)), crack tip asymmetry (Fig. 2(c)), or a combination of both (Fig. 2(d))

The effects of non-symmetry on the crack state and delamination growth of a non-symmetric crack in an FML are discussed in comparison with the symmetric crack configuration in the following subsections.

2.1. Effects on stress intensity factors of two crack tips

The stress state at a crack tip in a metallic panel can be characterized with the stress intensity factor experienced at the crack tip. According to Alderliesten [2, 3], the total stress intensity factor of the crack tip (K_{total}) in the metal layers of FMLs can be expressed based on the principle of superposition:

$$K_{total} = K_{ff} + K_{br} \tag{1}$$

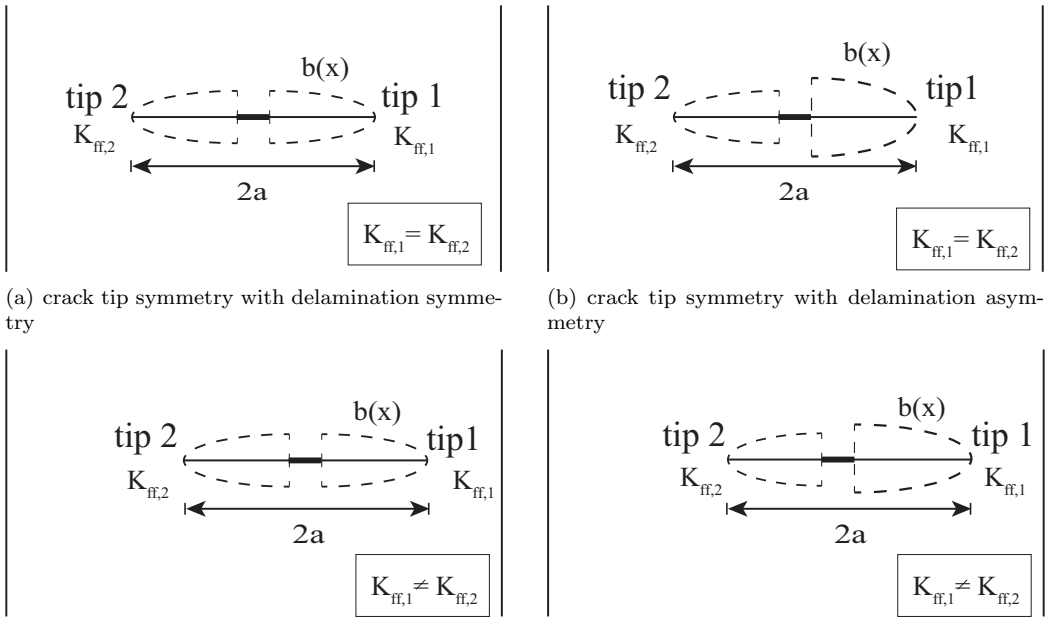

(a) crack tip symmetry with delamination symmetry

(b) crack tip symmetry with delamination asymmetry

(c) crack tip asymmetry with delamination symmetry

(d) crack tip asymmetry with delamination asymmetry

Figure 2: Comparison of symmetric and non-symmetric crack configurations in FMLs

in which K_{ff} is the stress intensity factor due to far-field stresses in metal layers and K_{br} is due to the bridging stress in intact bridging fibres. In other words, the load transfer from the cracked metal layer to the intact bridging fibres leads to a negative K_{br}, resulting in a smaller superposed stress intensity factor (K_{total}) experienced at the crack tip.

For two symmetric crack tips, the influence of free edge boundary conditions are the same, which leads to $K_{ff,1} = K_{ff,2}$. This symmetry is valid for the crack cases in Fig. 2(a) and Fig. 2(b). On the contrary, $K_{ff,1} \neq K_{ff,2}$ is valid for the cases of asymmetric crack tips in Fig. 2(c) and Fig. 2(d) [12, 20].

The symmetric delamination shapes for the symmetric crack tips in Fig. 2(a) lead to $K_{br,1} = K_{br,2}$ according to the study of Alderliesten [2]. Even though the K_{br} solution for non-symmetric delamination shapes are unknown yet, $K_{br,1} \neq K_{br,2}$ is expected as the difference in delamination shapes can lead to non-symmetric bridging stress distribution along the crack. Despite the symmetric delamination shapes in Fig. 2(c), $K_{br,1} \neq K_{br,2}$, as a result of non-symmetric crack opening displacement, which is explained in next subsections.

It is then obvious that K_{total} is only the same for two tips if there is both crack tip and delamination symmetry. Either crack tip asymmetry or delamination asymmetry could lead to different total stress intensity factors for two tips. Thus different crack growth behaviour of two tips of a non-symmetric crack is expected in an FML. The proposed model should be capable of analysing these phenomena.

2.2. Effects on crack opening displacement

It is well known that a symmetric crack in a metal panel possesses a symmetric crack opening displacement with respect to its crack centre under uniform tensile loading, and that the maximum crack opening occurs at the crack centre. For an FML under Mode I far-field loading, the stresses in the metal layers can be calculated with Classical Laminate Theory (CLT). The symmetric crack opening displacement of a central crack under applied load can then be determined [2, 3].

However, the crack opening of a non-symmetric crack in an FML under Model I loading needs to be re-analysed. The study in [20] found that a non-symmetric crack in a finite metallic panel has a larger

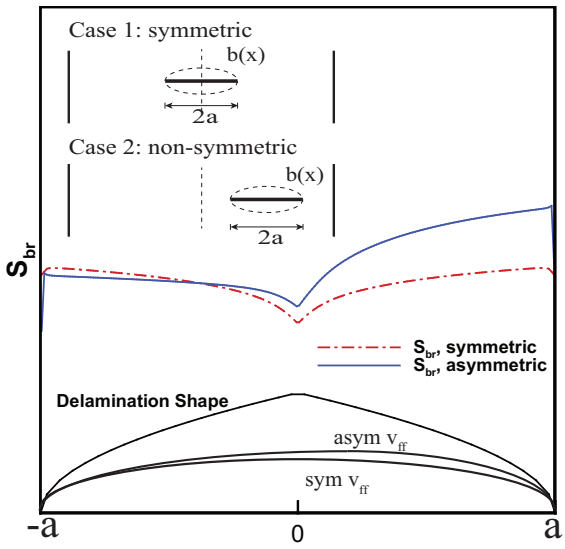

Figure 3: Illustration of bridging stress distributions for symmetric and non-symmetric crack cases [20]

crack opening displacement than a central crack with the same length. In addition, the presence of a non-symmetric crack eliminates the symmetry possessed by a centrally cracked panel, the crack opening contour of a non-symmetric crack is asymmetric.

The difference in the crack opening displacements of a symmetric crack and a non-symmetric crack in FMLs due to far-field stresses implies different bridging stress distributions in the intact bridging fibres along the crack, which affects both the delamination growth at the metal/composite interfaces and crack growth in the metal layers. The effects are discussed in detail in the next subsection.

2.3. Effects on load transfer from cracked metal layers to bridging fibres

The intact fibres in the wake of fatigue cracks restrain the crack opening in the metal layers in FMLs, which introduces load transfer from the cracked metal layers to the fibre layers. The load transfer is achieved by shear at the metal/composite interfaces resulting in interface delamination growth.

The load transfer between the two adherent substances is estimated by Alderliesten using the principle of displacement compatibility, i.e. the sum of the crack opening due to far-field load (V_{ff}) and crack closing due to the load transfer (V_{br}) should be equal to the deformation of fibre prepreg layers including shear deformation (δ_{pp}) and fibre elongation (δ_f) [2, 3]. See the following equation:

$$V_{ff}(x) - V_{br}(x) = \delta_{pp}(x) + \delta_f(x) \tag{2}$$

where V_{br} and δ_f are functions of bridging stress distribution in bridging fibres ($S_{br}(x)$) and V_{ff} and δ_{pp} are functions of far-field stresses in metal layers [2, 3].

The bridging stress distributions for a symmetric case and a non-symmetric case are compared in Fig. 3 in order to illustrate how the difference in the crack opening displacements of both crack scenarios affects the load transfer [20]. For the symmetric crack case with symmetric delamination shapes, all the variables in Eq. 2 are symmetric with respect to the crack centre, a symmetric bridging stress distribution in the bridging fibres can be calculated with Eq. 2 [2]. Symmetric crack growth and symmetric delamination growth in FMLs can be predicted as well with the approach in [2].

In contrast, the non-symmetric case with the same delamination shapes has asymmetric V_{ff}, see Fig. 3. A relatively larger crack opening for one crack tip than another results in higher bridging stress according to the principle of displacement compatibility, as illustrated in Fig. 3. The higher bridging stress distribution indicates a larger K_{br} for the corresponding crack tip. Meanwhile the higher bridging stress distribution

could promote larger delamination growth under fatigue loading, eventually resulting in a non-symmetric delamination shape. It is notable that the resultant K_{br} and K_{ff} are different, non-symmetric crack growth behaviours are therefore expected.

Based on the analysis, it can be argued that the crack tip asymmetry and delamination asymmetry interact with one another. A general crack configuration illustrated in Fig. 2(d) could be expected. The proposed model should be able to deal with the influence of non-symmetry resulting from both crack tip non-symmetry and the difference in delamination shapes.

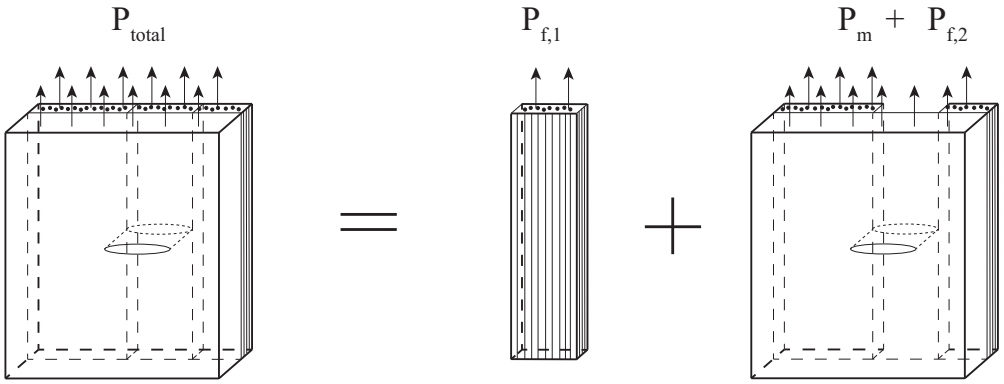

Figure 4: Decomposition of loads in FMLs system

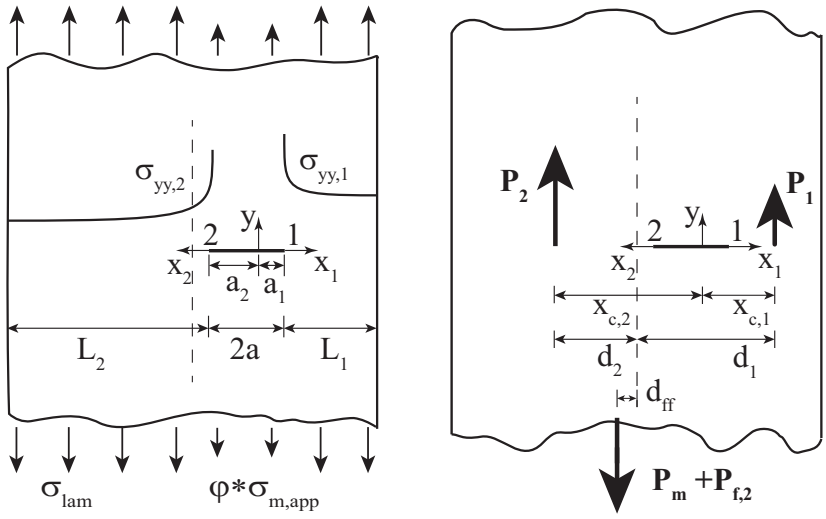

(a) actual stress distributions (b) equivalent loads

Figure 5: Illustration of equivalent loads for actual stress distributions

3. Model derivation

The general methodology that is based on LEFM, the principle of superposition and displacement compatibility used in [2, 3] for analysing symmetric cracks in FMLs can also be used for non-symmetric cracks. In comparison to symmetric cracks in FMLs, the physically different crack growth behaviour of non-symmetric cracks resulting from the asymmetric boundary conditions and difference in delamination shapes, however, need to be re-analysed. The core to this analysis is to calculate K_{ff} and K_{br} for each crack tip, and to derive

the asymmetric crack opening displacement and the corresponding load transfer (S_{br}) which associates the crack growth and delamination growth.

In order to aid in calculating K_{ff} and K_{br} for each crack tip, the far-field applied load is decomposed using the principle of superposition, see Fig. 4. The stresses carried by metal layers, $\sigma_{m,app}$, and composite layers, $\sigma_{f,app}$, of an FML under total applied load P_{total} or applied stress σ_{lam} can be calculated with CLT [9, 21]. Then the load transmitted by the metal layers, P_m, and loads transmitted by fibres over the total crack length, $P_{f,1}$, and the rest fibres, $P_{f,2}$, can be respectively expressed as:

$$P_m = n_m t_m \sigma_{m,app} W \tag{3}$$

$$P_{f,1} = n_f t_f \sigma_{f,app} 2a \tag{4}$$

$$P_{f,2} = n_f t_f \sigma_{f,app} (W - 2a) \tag{5}$$

where W is the width of the panel and $2a$ is the total crack length. The subscripts m and f refer to metal layer and fibre layer respectively. n and t indicate the number of layers and their thickness.

3.1. K_{ff} calculation

It is assumed that the stress distribution in front of a crack tip can be described with the Westergaard stress distribution in FMLs [11]. Since the non-symmetry results in different stress states at two crack tips of a non-symmetric crack, it is argued that the Westergaard stress distributions ahead of the two crack tips are different. [20]. The different stress distributions are illustrated in Fig. 5(a).

The Westergaard stress distribution artificially defines a half crack length with a maximum opening displacement at the root [20]. In order to achieve a continuous crack opening displacement for a non-symmetric crack calculated with two different Westergaard stress distributions, two different crack lengths (a_1, a_2) are assumed, instead of using the half crack length a of a crack with the length of $2a$ (Eqs. 6-7). This method has been applied for calculating stress intensity factors and crack opening of an eccentric crack in a metal strip and is explained in detail in [20]. Thus the corresponding stress distributions in front of two crack tips in an eccentrically cracked FML can be given by:

$$\sigma_{yy,1} = \frac{\sigma_1}{\sqrt{1 - (a_1/x_1)^2}} \tag{6}$$

$$\sigma_{yy,2} = \frac{\sigma_2}{\sqrt{1 - (a_2/x_2)^2}} \tag{7}$$

where σ_1 and σ_2 are laminate stresses to be determined for the two crack tips. a_1 and a_2 are the assumed two crack lengths whose sum should be the total crack length (Eq. 8) and the corresponding x_1, x_2 coordinates are illustrated in Fig. 5(a).

$$a_1 + a_2 = 2a \tag{8}$$

Additionally, the crack opening at the root of two half crack lengths described with the Westergaard stress distribution should be the same in order to fulfil the physics of the crack problem, which is given analytically by[20]:

$$\frac{\sigma_1 S}{E_m} a_1 = \frac{\sigma_2 S}{E_m} a_2 \tag{9}$$

where S is the matrix for calculating the stresses in the metal layers for a given laminate stress. This matrix for an FML with a symmetric layup subjected to uniform tensile far-field loading can be given by:

$$S = Q_m [A] t_{lam} \tag{10}$$

with Q_m being the stiffness matrix of the metal layers in laminate coordinates, $[A]$ being the extensional matrix of the ABD-matrix for a specific FML laminate and t_{lam} is the thickness [9, 21].

At the cracked section of the panel, the loads carried by the intact materials are then given by:

$$P_1 = \int_{a_1}^{a_1+L1} \sigma_{yy,1} \mathrm{d}x_1 \cdot t_{lam} \tag{11}$$

$$P_2 = \int_{a_2}^{a_2+L_2} \sigma_{yy,2} \mathrm{d}x_2 \cdot t_{lam} \tag{12}$$

where L_1 and L_2 are the lengths of intact strips as illustrated in Fig. 5(a).

These two loads and the far-field load (Fig. 5(b)) should not only satisfy load equilibrium but also moment equilibrium [20]:

$$P_1 + P_2 = P_m + P_{f,2} \tag{13}$$

$$(P_m + P_{f,2})d_{ff} + P_1 d_1 = P_2 d_2 \tag{14}$$

with d_{ff}, d_1 and d_2 being the distances between the corresponding equivalent loads and the vertical symmetric line of the laminate panel as illustrated in Fig.5(b). These distances can be calculated based on their geometric relations.

The equivalent loads (P_1, P_2) of the Westergaard stress distributions ($\sigma_{yy,1}$, $\sigma_{yy,2}$) illustrated in Fig. 5 should be located at their centroids, respectively ($x_{c,1}$, $x_{c,2}$) [20]:

$$x_{c,1} = \frac{\int_{a_1}^{a_1+L_1} \sigma_{yy,1} x_1 \mathrm{d}x_1}{\int_{a_1}^{w_1} \sigma_{yy,1} \mathrm{d}x_1} \tag{15}$$

$$x_{c,2} = \frac{\int_{a_2}^{a_2+L_2} \sigma_{yy,2} x_2 \mathrm{d}x_2}{\int_{a_2}^{w_2} \sigma_{yy,2} \mathrm{d}x_2} \tag{16}$$

According to their geometrical relationship, d_1 and d_2 can be given by:

$$d_1 = \frac{W}{2} - (L_1 + a_1 - x_{c,1}) \tag{17}$$

$$d_2 = \frac{W}{2} - (L_2 + a_2 - x_{c,2}) \tag{18}$$

The location of the equivalent load of the far-field stress after decomposition can also be calculated by:

$$d_{ff} = \frac{W}{2} - \frac{\int_0^{L_2} \sigma_{lam} x \mathrm{d}x + \int_{L_2}^{L_2+2a} \varphi\sigma_{m,app} x \mathrm{d}x + \int_{L_2+2a}^{W} \sigma_{lam} x \mathrm{d}x}{\int_0^{L_2} \sigma_{lam} \mathrm{d}x + \int_{L_2}^{L_2+2a} \varphi\sigma_{m,app} \mathrm{d}x + \int_{L_2+2a}^{W} \sigma_{lam} \mathrm{d}x} \tag{19}$$

where $\varphi\sigma_{m,app}$ denotes that $\sigma_{m,app}$ is recalculated based on the whole laminate thinkness, with φ being expressed as:

$$\varphi = \frac{n_m t_m}{t_{lam}} \tag{20}$$

Solving the system of Eqs. 6-19 provides the results for all the relevant unknown parameters. This prediction model is implemented in a numerical calculation model in the MATLAB language. After derivation the system of Eqs. 6-19 can be written as a nonlinear function of a_1. Although an analytical solution is extremely hard to obtain for the nonlinear function, a numerical method with a combination of bisection, secant and inverse quadratic interpolation methods is adopted to solve for the value of a_1. Then all other variables can be calculated.

The curing process for manufacturing FMLs causes thermal residual stresses in the laminate due to the mismatching thermal expansion coefficients between the metal sheets and fibre layers. The tensile thermal residual stress for metal layers ($\sigma_{m,cur}$) is regarded as far-field stress when the crack is present [2, 3]. It is therefore assumed in this paper that the boundary condition has the same effects on the crack behaviour

due to curing stress in metal layers as on the stress intensity factor due to far-field applied stress. Then the resultant stress intensity factors for the two crack tips can be expressed as:

$$K_{ff,1} = (\sigma_1 S + \frac{\sigma_1}{\sigma_{lam}}\sigma_{m,cur})\sqrt{\pi a_1} \tag{21}$$

$$K_{ff,2} = (\sigma_2 S + \frac{\sigma_2}{\sigma_{lam}}\sigma_{m,cur})\sqrt{\pi a_2} \tag{22}$$

3.2. Crack opening displacement derivation

The use of the Westergaard method provides the possibility of direct calculation of crack opening displacement [22, 23]. For a non-symmetric crack, the crack opening is calculated with two Westergaard functions defining two half crack lengths that is illustrated in Fig. 6 [20].

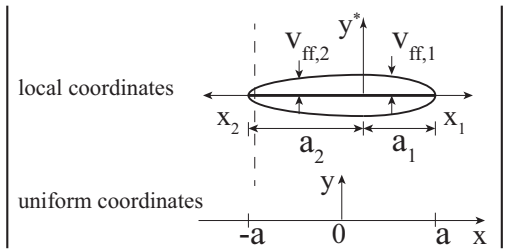

Figure 6: Illustration of crack opening displacement

The crack opening displacements for the two half cracks (Fig. 6) due to the applied far-field stress and curing stress can be given by:

$$v_{ff,1} = \frac{2(\sigma_1 S + \frac{\sigma_1}{\sigma_{lam}}\sigma_{m,cur})}{E_m}\sqrt{a_1^2 - x_1^2} \tag{23}$$

$$v_{ff,2} = \frac{2(\sigma_2 S + \frac{\sigma_2}{\sigma_{lam}}\sigma_{m,cur})}{E_m}\sqrt{a_2^2 - x_2^2} \tag{24}$$

It is notable that the derived crack opening displacements are in local coordinates (Fig. 6). They need to be mapped to a uniform coordinates with $x = 0$ located at the crack centre in order to calculate the bridging stress distribution with the Westergaard method, see Fig. 6. As the mapped COD cannot be expressed by one analytical equation, it is denoted as $V_{ff}(x)$ in this paper.

3.3. S_{br} calculation

It is believed that the same displacement compatibility between cracked metal layers and intact bridging fibre layers used by Alderliesten for the symmetric crack configuration [2, 3] can be used to calculate the bridging stress distribution for the non-symmetric crack configuration. Consider a generic damage configuration, illustrated in Fig. 7, where the delamination shape $b(x)$ and crack opening $V_{ff}(x)$ are asymmetric with respect to the crack centre. The dashed line in Fig. 7 represents a symmetric crack opening given as a reference.

Similar to the method in [8], the delamination shape is divided into bar elements. Due to the known issue that the magnitude of the calculated K_{br} is much more sensitive to the bridging stresses in the bridging fibres very close to the crack tip than those in other elements, the elements next to the crack tips are refined by assigning gradually smaller width, as shown in Fig. 7. Node x_i is the centre point of ith bar element where the bridging stress over width w_i is approximated by $S_{br}(x_i)w_i$ with $S_{br}(x_i)$ being the bridging stress at the node x_i.

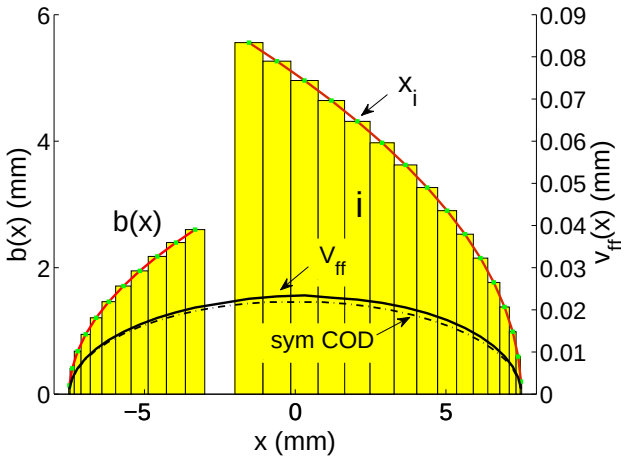

Figure 7: Illustration of delamination bars and crack opening

Eq. 2 can be used to calculate the S_{br} distribution along the crack flank. $V_{ff}(x)$ for any location x in a uniform coordinates with its origin at the crack centre has been calculated in the preceding subsection. $V_{br}(x)$ can be calculated with the equation as follows:

$$V_{br}(x) = \sum_{-a<x_i<a} V(x, x_i) \tag{25}$$

where $V(x, x_i)$ denotes the crack opening at x due to a pair of point loads at x_i of the ith element (Fig. 7). For a cracked panel under a pair of point loads illustrated in Fig. 8, the analytical solution has been provided by Tata et al. [23].

$$V(x, x_i) = \frac{1}{G(1+v)} \mathrm{Im}\bar{Z}_I - \frac{b(x_i)}{2G} \mathrm{Re} Z_I \tag{26}$$

where Z_I and $\bar{Z}_I$ are the Westergaad stress functions and $b(x_i)$ is the delamination length at x_i, detailed information is given in Appendix A.

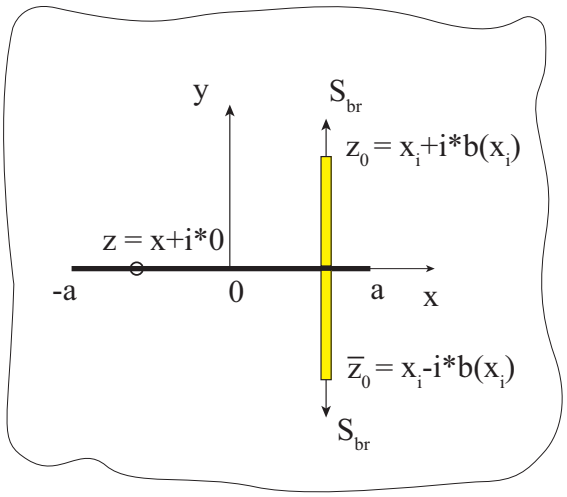

Figure 8: Two point bridging loads

The shear deformations of fibre layers for unidirectional plies and cross-ply layers have been calculated in [3], however the stress in the metal layers, S_{al} in the equations derived by Alderliesten, needs to be replaced by $\sigma_1 S + \frac{\sigma_1}{\sigma_{lam}}\sigma_{m,cur}$ or $\sigma_2 S + \frac{\sigma_2}{\sigma_{lam}}\sigma_{m,cur}$ for each half crack (a_1, a_2).

The fibre elongation can be calculated by

$$\delta_f(x) = \frac{S_f + S_{br}}{E} b(x) \tag{27}$$

where S_f is the sum of $\sigma_{f,app}$ and $\sigma_{f,cur}$ that is the curing stress in the fibre layers.

Due to the fact that $V_{br}(x)$ is related to the bridging stresses at all the elements, Eq. 2 has to be solved for all the bar elements simultaneously. A numerical solution can therefore be obtained [3].

$$S_{br}(x) = H^{-1}Q \tag{28}$$

where

$$H = \sum_{-a<x_i<a} \frac{V(x,x_i)}{S_{br}(x_i)} + \frac{b(x)}{E_f} \tag{29}$$

$$Q = V_{ff}(x) - \delta_{pp}(x) - \frac{S_f}{E_f} b(x) \tag{30}$$

3.4. K_{br} calculation

The bridging stress is defined in this paper as the stress acting in the fibre layers. However, this bridging stress needs to be recalculated for the stress acting in each metal layer in order to calculate the K_{br} for each crack tip. The recalculation is given as [3]:

$$S_{br,m}(x) = S_{br}(x)\frac{n_f t_f}{n_m t_m} \tag{31}$$

Then the stress intensity factor for each crack tip due to the bridging stress distribution can be calculated by:

$$K_{br,1} = \sum_{-a<x_i<a} \frac{S_{br,m}(x_i)w(x_i)}{2\sqrt{\pi a}} \Big[\sqrt{\frac{a+z_0}{a-z_0}} + \sqrt{\frac{a+\bar{z}_0}{a-\bar{z}_0}} - \alpha b(x_i)\Big(- \sqrt{\frac{a+z_0}{a-z_0}}\frac{a\cdot i}{(a+z_0)^2} + \sqrt{\frac{a+\bar{z}_0}{a-\bar{z}_0}}\frac{a\cdot i}{(a+\bar{z}_0)^2}\Big)\Big]$$

$$K_{br,2} = \sum_{-a<x_i<a} \frac{S_{br,m}(x_i)w(x_i)}{2\sqrt{\pi a}} \Big[\sqrt{\frac{a-z_0}{a+z_0}} + \sqrt{\frac{a-\bar{z}_0}{a+\bar{z}_0}} - \alpha b(x_i)\Big(\sqrt{\frac{a-z_0}{a+z_0}}\frac{a\cdot i}{(a-z_0)^2} - \sqrt{\frac{a-\bar{z}_0}{a+\bar{z}_0}}\frac{a\cdot i}{(a-\bar{z}_0)^2}\Big)\Big] \tag{32}$$

3.5. Crack growth model and delamination growth model

The fatigue crack growth rate in metal is predicted with the Paris relation after the stress intensity factor for each crack tip is obtained [3]:

$$\frac{da}{dN} = C_{cg}(K_{eff})^{n_{cg}} \tag{33}$$

where C_{cg} and n_{cg} are equation constants for Paris equation. For thin $2024-T3$ aluminium, the values are $C_{cg} = 2.17 \cdot 10^{-12}$ and $n_{cg} = 2.94$ [2, 3]. K_{eff} is related to the range of K_{total} and the stress ratio R [24]:

$$K_{eff} = (0.55 + 0.33R + 0.12R^2)(1-R)\cdot \Delta K_{total} \tag{34}$$

For delamination growth at the interface between metal layers and fibre layers, the strain energy release rate G instead of K is employed as the driving force, simply because it is easier to calculate G at the interface of dissimilar materials [2, 3]. The strain energy release rate for each delamination column can be given in terms of stresses in bridging fibres:

$$G = \frac{n_f t_f}{2jE_f}\left(\frac{n_m t_m E_m}{n_m t_m E_m + n_f t_f E_f}\right)(S_f(x) + S_{br}(x))^2 \tag{35}$$

Then the interface delamination can also be calculated using the Paris relation [3]:

$$\frac{db}{dN} = C_d(\sqrt{G_{max}} - \sqrt{G_{min}})^{n_d} \tag{36}$$

with C_d and n_d being the Paris parameters. For the fibre metal laminate Glare, the values are $C_d = 0.05$ and $n_d = 7.5$ [2, 3].

4. Experimental procedure

4.1. Material and manufacturing

The FML materials used for validation tests are composed of layers of S2-glass fibres reinforced FM94 epoxy resin prepreg and 2024-T3 aluminium, which is known as Glare. The lay-up of the specimens is [Al/0/90/Al/90/0/Al] with 90 and 0 referring to the orientation of the prepreg layers with respect to the rolling direction of the aluminium. Table 1 provides the properties of the constituents.

Table 1: Material properties [11]

	Al	**Prepreg**
Young's modulus $E_x[GPa]$	72.4	48.9
Young's modulus $E_y[GPa]$	72.4	5.5
Shear modulus $G_{xy}[GPa]$	27.6	5.55
Poisson's ratio v_{xy}	0.33	0.33
Poisson's ratio v_{yx}	0.33	0.0371
Thickness of single layer$[mm]$	0.4	0.133
Thermal expansion coefficient[1/℃]	$22 \cdot 10^{-6}$	$6.1 \cdot 10^{-6}(0°)$ $26.2 \cdot 10^{-6}(90°)$

The aluminium layers and cross-plies were stacked together according to the lay-up, and then were put into an autoclave for curing. The curing process was carried out with a maximum temperature of 120 ℃ and maximum pressure of 6 bars. Then the Glare laminates were milled into the specimen size described in Fig. 9.

4.2. Test matrix

In order to validate the proposed model for predicting non-symmetric fatigue crack growth in FMLs, the specimen configuration with initial non-symmetric saw-cuts that is illustrated in Fig. 9 was adopted. A circular hole with radius of 1.5 mm was applied to obtain saw-cuts from where the crack growth starts. The parameters of respective specimen configurations are given in Table. 2, which comprise the test matrix. That the length of a saw-cut is equal to the hole radius means no initial saw-cut is applied at the corresponding hole edge in order to get a delayed crack growth and corresponding delamination growth. A symmetric crack configuration (sym-1) was tested as a reference for comparison.

Table 2: Test matrix

Specimen	S_{hc} (mm)	$a_{1,s}$ (mm)	$a_{2,s}$ (mm)
sym-1	0	3	3
asym-1	0	7	1.5
asym-2	30	3	3

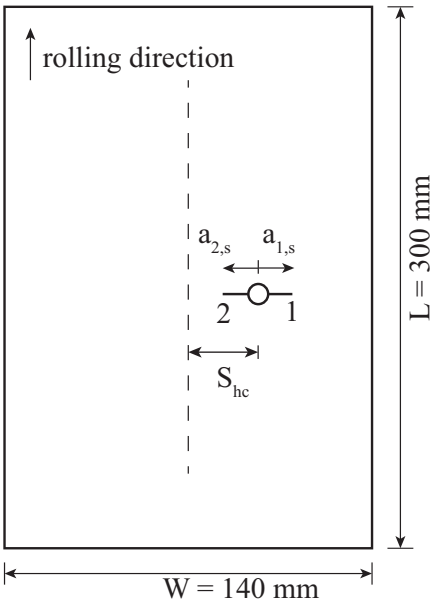

Figure 9: Specimen configuration

4.3. Fatigue test

The test set-up is shown in Fig. 10. A MTS 810 servo hydraulic test frame with a 250 kN load-cell (model 661.22D-01) was used. The specimen was mounted on the test frame with pin-hole grips such that no rotation constraints were applied. All the fatigue tests were done under constant amplitude cyclic loading under force control. The maximum applied stress level was 120 MPa, the stress ratio was $R = 0.05$ and the frequency was $f = 10\ Hz$.

Cameras were used during the fatigue tests to take pictures which were post-processed to obtain the crack length and delamination shape evolution. The test was suspended after a certain number of fatigue cycles and the maximum stress was applied in order to get the maximum displacement of the crack opening and maximum deformation of the specimen. After that cameras took pictures of both sides of the specimen (see Fig. 10). The test was then resumed. This process was iterated until enough crack lengths were obtained in the specimen.

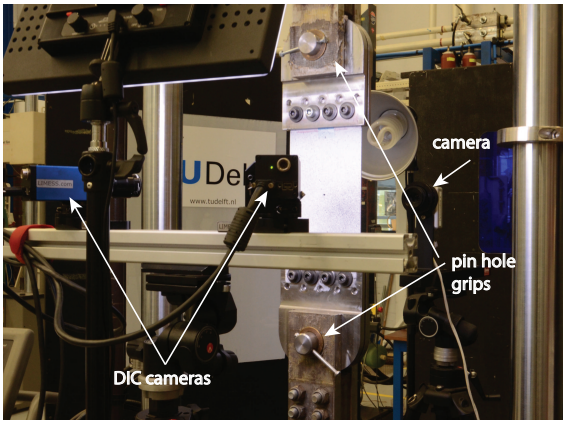

Figure 10: Test set up

A strip of millimeter paper was bonded to the surface of the specimen facing a high resolution camera.

The pictures captured by this camera were post-processed with ImageJ to obtain the crack lengths. The 7-point incremental polynomial method recommended in the ASTM E647-00 [25] was applied to derive crack growth rates with the crack lengths and corresponding cycles known.

The detection technique of the delamination shape adopted was the Digital Image Correlation (DIC) method [26–28]. The DIC method is known for measuring the strain distribution [26]. The DIC method obtains the deformation distribution by tracking the displacement of the random speckle patterns in the image of a deformed specimen under applied load and in the reference image of the specimen without any deformation. This displacement distribution is then processed to acquire the strain field. Due to the fact that the pieces of debonded aluminium carry negligible load while the bonded part still bears much more load, the evident difference in the strain distribution measured with DIC method between the delaminated part and bonded part makes the delamination front visible [27, 28].

In order to facilitate the correlation in the DIC method, the surface of the specimen had been painted random airbrushed black speckles with white background base coat of paint before the specimen was tested. The VIC-3D DIC system offered by Correlated Solutions was used to make the strain measurements. Two DIC cameras took the reference image and deformed images during fatigue testing. The image correlation was made with the subset size of $21 \cdot 21$ pixels and step of 5.

5. Model validation

The test data is used to validate the proposed model in this paper. Both the crack growth rates and the delamination shapes from the test and prediction are compared.

First the predicted crack growth rates are compared to the test results of specimen asym-1 (see Table. 2) in Fig. 11. The crack length is measured from the hole centre to the crack tip respectively. As can be seen the prediction correlates well with test data. The initial over prediction is due to the imprecise delamination shape assumed as input for the model [2, 3]. However, this over prediction vanishes after several cycles. Due to the non-symmetry, different crack lengths are obtained after fatigue test, this phenomenon is also captured by the prediction model as can be seen from the final predicted and tested crack lengths in Fig. 11.

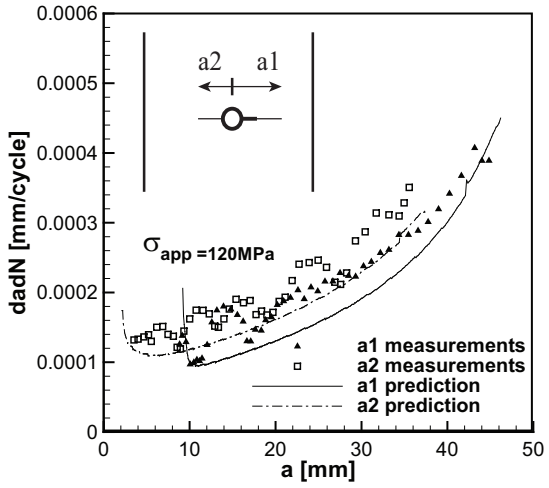

Figure 11: comparison of crack growth rates for specimen asym-1

Then the predicted and measured delamination shapes are compared for asym-1 in Fig. 12. The delamination shapes obtained with the DIC method at the end of testing are compared to the results obtained from etching the aluminium layers away to validate the DIC method, and the corresponding prediction results are also presented in Fig. 12. An image of the delamination shape and asymmetric crack lengths of specimen

asym-1 is shown in Fig. 13. The predicted delamination shapes are compared to the DIC measurements during the growth. Good correlation is observed.

The crack tip of $a1$ in asym-1 started growing at first from the saw-cut tip, another crack initiated at the hole edge after a while. Therefore the delamination shape for $a1$ (b1) is larger than that for $a2$ (b2) in the beginning. The difference in the delamination shapes decreases with fatigue life N until N is around 125500 cycles. Then the crack lengths are long enough so that the boundary condition affects more the crack growth and corresponding delamination growth. b1 is becoming bigger than b2 after this cycle number. This phenomenon is discussed in detail in Section 6.

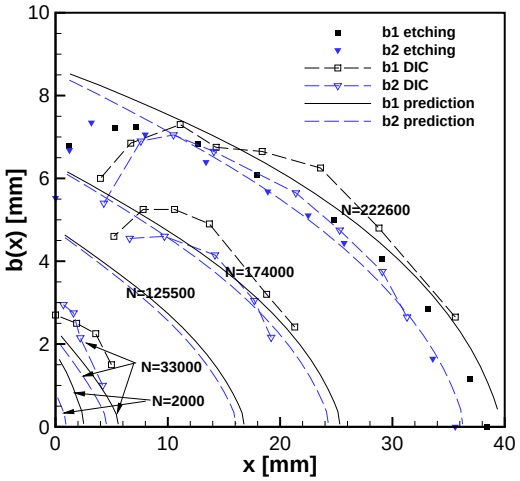

Figure 12: Delamination evolution for asym-1

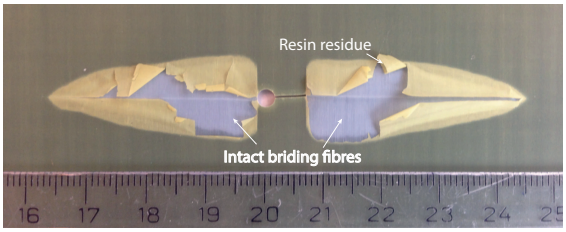

Figure 13: Delamination shape of specimen asym-1 after testing

Specific data comparison between the experiment and prediction is made to quantify the precision of the prediction model. This comparison is made in Table 3 for asym-1 specimen. As can be seen, for the crack growth prediction the average relative error is -0.168, which is quite acceptable. The high relative error can be attributed to the high scatter in experimental fatigue crack growth. For the delamination prediction the average relative error is -0.057. It can be conclude that the prediction method is quite accurate for the tested FML configurations.

The symmetric crack configuration, sym-1, is a special case of non-symmetric crack scenario. The prediction results together with test data for the symmetric case are given in Fig. 14. The corresponding data for asym-2 is also presented to highlight the effects of non-symmetric boundary condition on crack growth in FMLs. The crack length is measured from the hole centre to the crack tip as well. The cracks initiate at the two saw-cut tips simultaneously for two cases. Symmetric Sym-1 has same crack growth behaviour for the two crack tips. For asym-2, the crack growth rates of the two crack tips are the same for the crack length less than 10 mm where the boundary condition hardly affects the crack growth. Then the effects of boundary condition prevail. The crack tip relatively closer to the free edge grows faster than the

Table 3: Data comparison between the experiment and prediction for asym-1 specimen

category	length	experimental data	prediction	relative error
a1	15.5612381	0.000167866	0.000111	-0.338758577
	25.74909524	0.000215804	0.000163	-0.244683492
	30.23714286	0.00023775	0.000193	-0.188222923
	40.2356606	0.000341709	0.000304	-0.110353866
a2	8.116238095	0.000137232	0.000113	-0.176577749
	18.99190476	0.000167813	0.000156	-0.070391061
	28.26885714	0.000228018	0.000214	-0.061477015
	35.55468831	0.000350618	0.000296	-0.155775815
				average: -0.168
b1	7.157	7.2455	7.8807	0.087668208
	17.981	6.092	6.4747	0.062820092
	33.137	2.841	3.3114	0.165575502
b2	7.988	7.0565	7.4321	0.053227521
	18.906	5.6805	5.7007	0.003556025
	25.699	4.438	4.305	-0.029968454
				average: -0.057

other one.

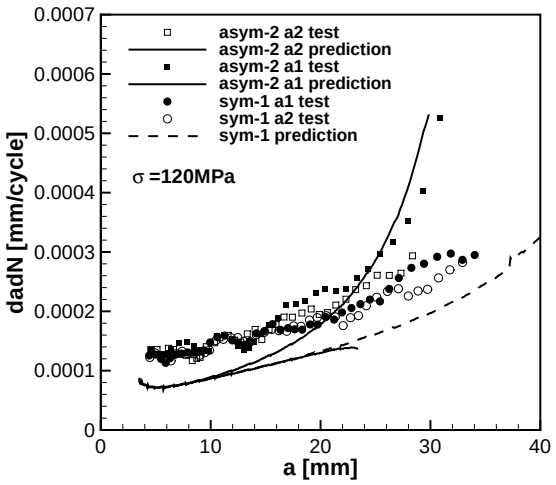

Figure 14: Comparison of crack growth rates for sym-1 and asym-2

6. Discussion

6.1. The catch-up phenomenon for non-symmetric crack growth in FMLs

From Fig. 12 it can be seen that the size of delamination shape b2 catches up with b1 during the short crack growth where the boundary condition effects are limited. This evolution of delamination damage interacts with the crack growth in metal layers. It can also be seen that the crack length bridged by b2 also catches up with the crack length bridged by b1 from Fig. 15 where the crack length measured from the saw-cut tip is plotted against the crack growth life N. The predicted crack growth rates presented in the same figure showed higher crack growth rate for $a2^*$ with smaller delamination b2 than $a1^*$ with lager delamination b1 in the beginning phase of the crack growth life.

As can be read from Table. 4, the calculated far-field stress intensity factors for the two crack tips are very close for the life period from $N = 2000$ to $N = 33000$. This is attributed to the fact that the crack lengths are still small enough so that the boundary condition effects are almost absent. Whereas the stress intensity factor due to bridging for $a2^*$ is smaller, because the smaller delamination shape b2 provides smaller bridging compared to the larger b1 for $a1^*$. This results in a higher total stress intensity factor for $a2^*$ according to Eq. 1, resulting in a faster crack growth and accompanying delamination growth.

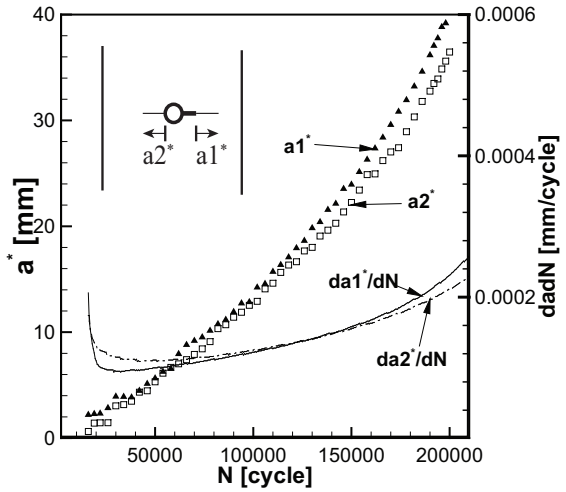

Figure 15: Illustration of catch-up phenomenon

Table 4: Variation of stress intensity factors

N	$K_{ff,1}$	$K_{ff,2}$	$K_{br,1}$	$K_{br,2}$
2000	702.96	703.24	237.95	227.74
33000	876.33	876.39	459.87	444.23
125500	1324.06	1318.76	848.61	843.67
174000	1622.4	1603.17	1089.86	1082.81
222600	2200.68	2085.52	1506.81	1468.67

As can be seen in Fig. 15 $a1^*$ grows faster than $a2^*$ after the crack length exceeds 10 mm, where the effects of boundary conditions override the effects of the bridging mechanism on the crack growth behaviour. The calculated stress intensity factors in Table. 4 further explain this.

6.2. Implementation of the proposed model for predicting MSD in FMLs

The present authors of this paper have already detailed a philosophy for predicting multiple-site damage growth behaviour in FMLs in [10]. The philosophy requires the ability to predict the crack interaction effects in terms of the load redistribution mechanism, and the ability to predict the crack growth with asymmetric delamination shapes and asymmetric boundary conditions for two crack tips in metal layers in FMLs. The load redistribution mechanism in FMLs as a result of stiffness variation has been studied with the precursor model proposed in [11], and the prediction model of non-symmetric crack growth in FMLs is proposed in this paper. Since the model proposed in this paper uses the Westergaard stress distributions to characterize the stress distribution ahead of a crack tip, the load redistribution due to stiffness variation caused by the presence of another crack can therefore be modelled [11]. These two models will be integrated to predict the crack growth behaviour in FMLs with MSD scenario.

6.3. Limitations of the proposed model

From Fig. 14, it is observed that the predicted crack growth rate for the tip very close to the free edge is a little over predicted at the last period of fatigue crack growth in asym-2, while the prediction for the other tip relatively far away from the free edge ahead is underestimated. This inaccuracy originates from the methodology used in Section 3 to calculate the far-field stress induced stress intensity factors for two crack tips and the asymmetric crack opening contour of a non-symmetric crack. The methodology is based on the model proposed in [20], which anaylses the deformation behaviour in a 2-dimensional metallic panel damaged by an eccentric crack.

The model in [20] has assumed that the Westergaard stress distribution and associated crack opening solution are applicable to non-symmetric crack tips. And two half crack lengths are defined as the lengths between the maximum crack opening location and the crack tips respectively. These assumptions are valid for most eccentric crack scenarios. For a crack case with a normalized crack length, the ratio of half crack length to the sum of half crack length and the ligament length, larger than 0.7, the assumptions lead to percent errors larger than 10% in predicted correction factors for stress intensity factors. The relative errors are obtained by comparing the prediction results with the results from the Isida method [12, 23]. The trend of the inaccuracy is already shown in [20]. This calculation error could result in a cumulative error in terms of fatigue crack growth life.

7. Conclusion

An analytical model has been developed to analyse the non-symmetric crack growth in FMLs. The non-symmetric crack growth in the metal layers and induced non-symmetric growth of delamination shapes at the composites/metal interfaces in FMLs were investigated in detail. The accuracy of the analytical model has been validated through comparing predictions with experimental data for several non-symmetric crack cases. Good correlation is observed.

Both the stress intensity factor due to the far-field loading (K_{ff}) and the stress intensity factor due to the bridging stress distributions (K_{br}) determine the non-symmetric fatigue crack growth in metal layers of FMLs. Implementation of these two stress intensity factor solutions requires analysis of two sorts of non-symmetries: crack tip non-symmetry and delamination shape non-symmetry. For small cracks, the delamination shape non-symmetry dominates the crack growth behaviour. When the crack length is long enough, the free edge boundary conditions will prevail and the crack growth behaviour is then dominated by the crack tip non-symmetry.

The load redistribution from the cracked metal layers to the intact fibre layers can only be solved on the condition of knowing the far-field loading induced crack opening behaviour of the eccentrically cracked metal layers. The proposed model is capable of analysing the deformation behaviour and calculating the bridging stress distribution of arbitrary delamination shape for non-symmetric fatigue crack growth in FMLs. The proposed model also provides the stress distribution in front of the crack tip, which can be utilized to analyse the effects of load redistribution due to stiffness variation in front of the crack tip on the crack state, such as the presence of other collinear cracks.

Acknowledgements

The authors are grateful to the Chinese Scholarship Council for financial support.

Appendix A.

The Westergaard stress functions for cracked body under two-point loads (see Fig. 8) are given by:

$$Z_I = \frac{P}{2\pi\sqrt{z^2-a^2}}(Part1 - i\cdot\alpha y_0 Part2) \tag{A.1}$$

where

$$Part1 = \frac{\sqrt{a^2 - z_0^2}}{z - z_0} + \frac{\sqrt{a^2 - \bar{z}_0^2}}{z - \bar{z}_0} \tag{A.2}$$

$$Part2 = \frac{\sqrt{a^2 - z_0^2}}{(z - z_0)^2} - \frac{\sqrt{a^2 - \bar{z}_0^2}}{(z - \bar{z}_0)^2} - \frac{z_0}{\sqrt{a^2 - z_0^2}(z - z_0)} + \frac{\bar{z}_0}{\sqrt{a^2 - \bar{z}_0^2}(z - \bar{z}_0)} \tag{A.3}$$

$$\alpha = \frac{1}{2}(1 + v) \tag{A.4}$$

and

$$\bar{Z}_I = \frac{P}{\pi}(Part3 - \alpha y_0 Part4) \tag{A.5}$$

where

$$Part3 = tan^{-1}(\sqrt{\frac{a + z_0}{a - z_0}}\sqrt{\frac{z - a}{z + a}}) + tan^{-1}(\sqrt{\frac{a + \bar{z}_0}{a - \bar{z}_0}}\sqrt{\frac{z - a}{z + a}}) \tag{A.6}$$

$$Part4 = \frac{1}{1 + \frac{a + z_0}{a - z_0}\frac{z - a}{z + a}}\sqrt{\frac{z - a}{z + a}}\sqrt{\frac{a - z_0}{a + z_0}}\frac{i \cdot a}{(a - z_0)^2} - \frac{1}{1 + \frac{a + \bar{z}_0}{a - \bar{z}_0}\frac{z - a}{z + a}}\sqrt{\frac{z - a}{z + a}}\sqrt{\frac{a - \bar{z}_0}{a + \bar{z}_0}}\frac{i \cdot a}{(a - \bar{z}_0)^2} \tag{A.7}$$

In these functions, P represents the point load per unit thickness, and the complex numbers z_0 $(x_0 + i \cdot y_0)$, $\bar{z}_0$ $(x_0 - i \cdot y_0)$ indicate the locations of the applied point loads in a xy-coordinates; z $(x + i \cdot y)$ indicates the location of interest in the same coordinates (Fig. 8).

For the application in this paper, the following substitutions are needed:

$$z = x + i \cdot 0 \tag{A.8}$$

$$z_0 = x_i + i \cdot b(x_i) \tag{A.9}$$

$$\bar{z}_0 = x_i - i \cdot b(x_i) \tag{A.10}$$

References

[1] A. Vlot, J. W. Gunnink, Fibre Metal Laminates-An Introduction, Kluwer Academic Publisher, Dordrecht, The Netherlands, 2001.

[2] R. Alderliesten, Analytical prediction model for fatigue crack propagation and delamination growth in Glare, International Journal of Fatigue 29 (2007) 628–646.

[3] R. C. Alderliesten, Fatigue crack propagation and delamination growth in Glare, Ph.D. thesis, Delft University of Technology, Delft, the Netherlands (2005).

[4] Q. Liu, J. Ma, L. Kang, G. Sun, Q. Li, An experimental study on fatigue characteristics of cfrp-steel hybrid laminates, Materials & Design 88 (2015) 643 – 650. doi:http://dx.doi.org/10.1016/j.matdes.2015.09.024.
URL `http://www.sciencedirect.com/science/article/pii/S0264127515304330`

[5] S. Khan, Fatigue crack and delamination growth in fibre metal laminates under variable amplitude loading, Ph.D. thesis, Delft University of Technology, Delft, the Netherlands (2013).

[6] S. U. Khan, R. C. Alderliesten, C. D. Rans, R. Benedictus, Application of a modified wheeler model to predict fatigue crack growth in fibre metal laminates under variable amplitude loading, Engineering Fracture Mechanics 77 (9) (2010) 1400–1416.

[7] S. U. Khan, R. C. Alderliesten, R. Benedictus, Delamination in fiber metal laminates (Glare) during fatigue crack growth under variable amplitude loading, International Journal of Fatigue 33 (9) (2011) 1292–1303.

[8] G. Wilson, Fatigue crack growth prediction for generalized fiber metal laminates and hybrid materials, Ph.D. thesis, Delft University of Technology, Delft, the Netherlands (2013).

[9] J. J. Homan, Fatigue initiation in fibre metal laminates, International Journal of Fatigue 28 (4) (2006) 366–374.

[10] W. Wang, C. Rans, R. C. Alderliesten, R. Benedictus, Philosophy of multiple-site damage analysis for fibre metal laminate structures, in: 28th Symposium of the International Committee on Aeronautical Fatigue (ICAF 2015), Helsinki, Finland, 2015, pp. 510–520.

[11] W. Wang, C. Rans, R. C. Alderliesten, R. Benedictus, Predicting the influence of discretely notched layers on fatigue crack growth in fibre metal laminates, Engineering Fracture Mechanics 145 (2015) 1–14.

[12] M. Isida, Stress-intensity factors for the tension of an eccentrically cracked strip, Journal of Applied Mechanics 33 (3) (1966) 674–675, 10.1115/1.3625138.

[13] M. Isida, On the determination of stress intensity factors for some common structural problems, Engineering Fracture Mechanics 2 (1) (1970) 61–79.
[14] D. L. Ball, The development of mode i, linear-elastic stress intensity factor solutions for cracks in mechanically fastened joints, Engineering Fracture Mechanics 27 (6) (1987) 653–681.
[15] D. L. Chen, B. Weiss, R. Stickler, A new approach for the determination of stress intensity factors for finite width plate, Engineering Fracture Mechanics 48 (4) (1994) 561–571.
[16] J. Grandt, A. F., Stress intensity factors for some through-cracked fastener holes, International Journal of Fracture 11 (2) (1975) 283–294.
[17] X. He, M. Tan, J. T. Xing, An investigation on fatigue crack growth rates through a designed nonsymmetric crack growth test, Engineering Fracture Mechanics 96 (0) (2012) 510–527.
[18] W. Qizhi, The crack-line stress field method for analysing sifs of strips-illustrated with an eccentrically cracked tension strip, International Journal of Fracture 59 (2) (1993) R39–R43.
[19] D. Stefanescu, L. Edwards, M. E. Fitzpatrick, Stress intensity factor correction for asymmetric through-thickness fatigue cracks at holes, International Journal of Fatigue 25 (7) (2003) 569–576.
[20] W. Wang, Multiple-site damage crack growth behaviour in fibre metal laminate structures, Ph.D. thesis, Delft University of Technology, Delft, the Netherlands (2017).
[21] S. Spronk, I. Şen, R. Alderliesten, Predicting fatigue crack initiation in fibre metal laminates based on metal fatigue test data, International Journal of Fatigue (0) (2014) –. doi:http://dx.doi.org/10.1016/j.ijfatigue.2014.07.004.
URL http://www.sciencedirect.com/science/article/pii/S014211231400187X
[22] H. Westergaard, Bearing pressure and cracks., Journal of Applied Mechanics 6 (1939) 49–53.
[23] H. Tada, P. C. Paris, G. R. Irwin, The stress analysis of cracks handbook, ASME, New York, 2000.
[24] J. Schijve, Fatigue of structures and materials, Springer, Dordrecht, The Netherlands, 2008.
[25] E647-00, ASTM, Standard test method for measurement of fatigue crack growth rates (2011).
[26] H. Lemmen, R. C. Alderliesten, R. Benedictus, J. Hofstede, R. Rodi, The power of digital image correlation for detailed elastic-plastic strain measurements, in: WSEAS International Conference on ENGINEERING MECHANICS, STRUCTURES, ENGINEERING GEOLOGY, WSEAS Press, Crete Island, Greece, (2008), p. 7389.
[27] R. Rodi, R. C. Alderliesten, R. Benedictus, Crack-tip behavior in fiber/metal laminates by means of digital-image correlation, Journal of Aircraft 47 (5) (2010) 1636–1646.
[28] Y. Huang, J. Liu, X. Huang, J. Zhang, G. Yue, Delamination and fatigue crack growth behavior in fiber metal laminates (Glare) under single overloads, International Journal of Fatigue 78 (2015) 53–60.